0026-895X/94/010199-12$03.00/0

MOLECULAR PHARMACOLOGY, 46:199-211, 1994.

Pattern Recognition Classification of the Site of Nephrotoxicity Based on Metabolic Data Derived from Proton Nuclear Magnetic Resonance Spectra of Urine

M. L. ANTHONY, B. C. SWEATMAN, C. R. BEDDELL, J. C. LINDON, and J. K. NICHOLSON

Department of Chemistry, Birkbeck College, University of London, London WC1H OPP, UK (M.L.A., J.K.N.), and Department of Physical Sciences, Wellcome Research Laboratories, Beckenham, Kent BR3 3BS, UK (B.C.S., C.R.B., J.C.L.)

Received December 3, 1993; Accepted March 25, 1994

SUMMARY

The computer-based pattern recognition procedures of nonlinear mapping and principal-component analysis have been applied to analyze ^{1}H NMR-generated metabolic data on the biochemical effects of 15 acute nephrotoxin treatments affecting the renal cortex and/or renal medulla in rats. The ^{1}H NMR signal intensities for 16 urinary metabolites representative of several major intermediary biochemical pathways were estimated using either a simple semiquantitative scoring system or complete peak intensity quantitation. NMR-derived data were treated as input coordinates in a multidimensional metabolic space and were analyzed by pattern recognition methods through which the dimensionality was reduced for display and categorization purposes. Different nephrotoxin treatments were initially classified using semiquantitative metabolite scores on the basis of their ^{1}H NMR-detectable biochemical effects, and a good separation of renal cortical toxin treatments from renal medullary toxin treatments was achieved. The refinement of using exact peak heights rather than metabolic data scores utilized the available metabolic information more fully and provided a unique classification of each type of toxin according to its pattern of biochemical effects and site of toxic action. Principal-component analysis provided consistently better results than did nonlinear mapping in terms of discrimination between different sites of toxicity, and maps generated from correlation matrices gave improved discrimination, compared with those based directly on the original metabolic data. A comparison between the use of an added internal quantitation standard (3-trimethylsilyl-[2,2,3,3-$^2H_4$]-1-propionate) and independently determined glucose excretion rates for scaling to the NMR-detected urinary glucose levels demonstrated that the consistent classification of site-specific nephrotoxicity was independent of the quantitation standard used. This study has provided a rigorous assessment of data processing, relative quantitation, and pattern recognition methods, and the utility of applying these methods to the classification of NMR-derived toxicological data. The considerable potential of the NMR-pattern recognition approach in the assessment of nephrotoxicity has also been confirmed with the discovery of new combinations of molecular markers of renal cellular damage.

^{1}H NMR spectroscopy of biofluids provides important information on the relative concentrations of biologically important low molecular weight metabolites and their dynamic physicochemical interactions in solution (1). Examination of ^{1}H NMR spectra of urine from animals with toxin-induced metabolic disorders has indicated that much of the information necessary to classify and biochemically assess experimental toxicity states is conveyed in the overall pattern of the metabolite resonances (2). However, the complexity of the ^{1}H NMR spectra have required the use of powerful methods of data reduction and analysis to gain the maximum amount of biochemical information from the spectra (1). Computer-based PR data reduction and mapping techniques such as NLM and PCA can be used to reduce the dimensionality of spectral data to a more readily interpretable form. In the application of these techniques to NMR-generated toxicity data, a series of objects (the ^{1}H NMR spectra of urine from individual animals) are examined with coordinates given by measurements of each of n descriptors (metabolites), thereby yielding an n-dimensional metabolite space that reflects the perturbed metabolite profile and hence the toxicity state of each individual animal. NLM techniques produce two- or three-dimensional diagrams in which the distances between the objects are obtained by a least-squares minimization fit to the interpoint distances in the

We thank the Science and Engineering Research Council and the Wellcome Foundation Ltd. for financial support (to M.L.A.) and the Wellcome Trust for current grant support (to M.L.A.).

ABBREVIATIONS: PR, pattern recognition; BEA, 2-bromoethanamine hydrochloride; CPH, cephaloridine; CrO_4^{2-}, sodium chromate; DCVHC, *S*-(1,2-dichlorovinyl)-L-homocysteine; DMG, *N,N*-dimethylglycine; GER, glucose excretion rate; HCBD, hexachloro-1,3-butadiene; HB, 3-D-hydroxybutyrate; Hg^{2+}, mercury(II) chloride; NLM, nonlinear map; 2-OG, 2-oxoglutarate; PAP, 4-aminophenol; PC, principal component; PCA, principal-component analysis; PI, propylene imine; TCTFP, 1,1,2-trichloro-3,3,3-trifluoro-1-propene; TSP, 3-trimethylsilyl-[2,2,3,3-$^2H_4$]-1-propionate; UN, uranyl nitrate.

original n-space (3). PCA derives linear combinations, i.e., PCs of the original variables (in this case NMR-generated metabolite values), such that (i) each PC is orthogonal (uncorrelated) with all other PCs and (ii) the first PC contains the largest part of the variance of the data set (information content), with subsequent PCs containing correspondingly smaller amounts of variance (4, 5). Therefore, a plot of the first two PCs produces a map in which the coordinates of the objects are derived from the two components that reproduce the most variance. Therefore PR methods can reduce the complexity of the NMR data sets and allow visualization of metabolic and toxicological patterns within the data.

We have previously described the application of NLM and PCA techniques to the classification of the acute toxicity of several nephrotoxins causing histologically detectable lesions to the renal medulla or renal cortex (more specifically, to the S_1 and S_3 segments of the proximal tubule), using a simple seven-level scoring system (6, 7) based on the levels of ^1H NMR-detected endogenous metabolites. Metabolites were selected for measurement on the basis of their ubiquitous appearance in ^1H NMR spectra of urine and their known importance in several key, intermediary, biochemical pathways. Excretion data were scored either as a function of time, which reflected the pharmacokinetic effects of the nephrotoxin treatments on metabolite excretion, or in terms of their maximum effect, i.e., the greatest changes induced in the excretion of any one metabolite by each nephrotoxin treatment (7). This mapping approach proved robust to the addition of NMR data for toxins that targeted different tissues (the liver and testes), as well as for different doses, sex influences, and nutritional influences (7).

The overall objective of the present study was to evaluate the scope and limitations of applying computer-based PR methods for the analysis and interpretation of metabolic data produced by ^1H NMR urinalysis studies of acute nephrotoxicity states. The original nephrotoxin data set described previously (6, 7) has been fully quantitated (from metabolite ^1H NMR peak height measurements) and augmented with scored and quantitated NMR urinalysis data derived from rats exposed to additional S_3 segment-directed proximal tubular nephrotoxins, including DCVHC, TCTFP, and UN, or the S_1/S_2 segment-directed proximal tubular nephrotoxin CPH, and the PR methods have been compared for semiquantitative and quantitative data. In addition, we have used the metabolic information present in ^1H NMR spectra from nephrotoxin-treated rats more efficiently by extending our strategy to incorporate analysis of quantitative data to examine the effects of different quantitation standards on the PR observations. Although TSP is frequently used as a chemical shift reference and quantitation standard, its use for quantitation has been considered to be flawed due to its ability to bind to protein, with consequent line broadening (1, 8). Because rats are physiologically proteinuric and nephrotoxin administration may exacerbate this (2), TSP-derived determinations were also validated by the use of independently determined GER data, using the ^1H NMR-detected glucose signal for internal standardization. The development and optimization of the NMR-PR approach described here have confirmed its potential value in the routine assessment and biochemical classification of acute toxicity processes.

Materials and Methods

Animals and treatments. Fifty-four male Fischer 344 rats (200–250 g; Harlan Olac) were placed individually in plastic metabolism cages and allowed free access to food and tap water. Rats were housed in well ventilated animal rooms with regular light cycles (12 hr of light, from 7 a.m. to 7 p.m.). After an acclimatization period of 2 days, rats were dosed with a range of nephrotoxins with different sites and mechanisms of action (see Table 1). Urinary volume and pH were measured and urine was centrifuged at 3000 rpm for 10 min at 4°, to remove food particles and other debris. Urine was then snap frozen using liquid nitrogen and was maintained at −20° before NMR measurements.

^1H NMR analysis of rat urine. Measurements were made at ambient probe temperature (298 ± 1°K) on Bruker AM400 and JEOL GSX500 spectrometers operating at ^1H frequencies of 400 and 500 MHz, respectively. Urine was analyzed after lyophilization and a standardized reconstitution step designed to correct for variations in urinary filtration rate between individuals (2). All urine samples were reconstituted in ^2H_2O (0.75 ml) containing TSP (1 mM) (δ 0.0). For each sample, 64 free induction decays were collected into 16,384 computer points using 45-degree pulses, a spectral width of 5000 Hz, an acquisition time of 1.7 sec, and an additional delay of 3.0 sec between pulses to allow T_1 relaxation. An exponential apodization function equivalent to a line broadening of 0.7 Hz was applied before Fourier transformation to improve signal-to-noise ratios. Water suppression was achieved by gated secondary irradiation at the water resonance frequency (off during acquisition). Resonance assignments were made by reference to the literature (1, 2), comparison of chemical shift and spin-spin coupling patterns, pH dependence of chemical shifts, and use of appropriate two-dimensional experiments (1) and were confirmed by standard additions where appropriate.

Semiquantitative analysis and scoring of ^1H NMR-generated data. ^1H NMR spectra of urine from rats administered CPH, DCVHC, TCTFP, or UN (5 and 20 mg/kg) were compared with spectra obtained at the same time point from untreated control animals, plotted on the same vertical scale. Changes in the ^1H NMR signal intensities for 16 selected endogenous metabolites (see Table 2) were derived by using the seven-level scoring system described previously (6, 7), as follows: +3, major elevation in signal intensity corresponding to >3 times the

TABLE 1

Doses and vehicles used for nephrotoxin administration in ^1H NMR toxicity studies and lesion site classifications

Urine collection times were −24–0 h before nephrotoxin administration and 0–8, 8–24, and 24–48 hr after dosing. All treatments were administered by intraperitoneal injection except CrO_4^{2-}, which was administered subcutaneously.

Treatment	Number of rats	Dose	Vehicle
Control	9	0 mg/kg	Saline/corn oil
S_1 segment proximal tubular nephrotoxin			
CrO_4^{2-}	2	20 mg/kg	Saline
S_1/S_2 segment proximal tubular nephrotoxin			
CPH	3	375 mg/kg	Saline
CPH	3	750 mg/kg	Saline
CPH	3	1500 mg/kg	Saline
S_3 segment proximal tubular nephrotoxins			
DCVHC	3	40 mg/kg	Saline
HCBD	3	200 mg/kg	Corn oil
Hg^{2+}	2	2 mg/kg	Saline
PAP	3	100 mg/kg	Saline
TCTFP	3	20 mg/kg	Corn oil
TCTFP	3	40 mg/kg	Corn oil
UN	3	5 mg/kg	Saline
UN	3	10 mg/kg	Saline
UN	3	20 mg/kg	Saline
Renal medullary nephrotoxins			
BEA	3	250 mg/kg	Corn oil
PI	5	20 μl/kg	Corn oil

TABLE 2
Metabolite ^{1}H NMR signals used in quantitative urinalysis studies

Metabolite	Signal measured	Multiplicity	Chemical shift
			δ
Acetate	CH_3	Singlet	1.94
Alanine	CH_3	Doublet	1.48
HB	CH_3	Doublet	1.20
Creatinine	CH_3	Singlet	3.02
Citrate	$(CH_2)_2$	AB	2.55
Glucose[a]	α-CH	Doublet	5.25
Glutamine	γ-CH_2	Multiplet	2.40
2-OG	CH_2	Triplet	2.47
Hippurate[b]	$(CH)_2$	AA′BB′	7.85
Lactate	CH_3	Doublet	1.33
Succinate	$(CH_2)_2$	Singlet	2.45
Trimethylamine-*N*-oxide	$(CH_3)_3$	Singlet	3.27
Valine	CH_3	Doublet	0.96
Dimethylamine	$(CH_3)_2$	Singlet	2.71
Lysine	δ-CH_2	Multiplet	1.71
DMG	$(CH_3)_2$	Singlet	2.89

[a] Total glucose was estimated from the α-anomeric proton resonance, assuming the normal ratio of α to β anomers of 36:64.
[b] The larger of the peaks (i.e., at the listed chemical shift) was used for the measurement.

individual control level; +2, significant elevation in concentration corresponding to 2–3 times control; +1, detectable but minor elevation in concentration of <2 times control; 0, not detectably different from control; −1, minor reduction in NMR signal intensity (up to 50% reduction from the comparable control signal intensity); −2, moderate reduction in NMR signal intensity (50–90% reduction from the comparable control signal intensity); −3, NMR signals of metabolite not detectable although detected in control.

Modal scores for each of the 16 metabolites from rats given BEA, CrO_4^{2-}, HCBD, Hg^{2+}, PAP, PI, or UN (10 mg/kg) were obtained from previously published data (7). The modal scores for each metabolite for each animal treatment group were used to construct a time-course data set containing information on the effects of the toxin treatments on the metabolite signal intensities at each individual postdosing time point (i.e., 0–8, 8–24, and 24–48 hr). A data set was compiled from this to describe the maximum change produced by each toxin treatment over 48 hr, corresponding to the most positive or negative modal score in the time-course data set. If this occurred more than once over 48 hr, the earliest value was recorded.

Generation of quantitative ^{1}H NMR peak intensity data. ^{1}H NMR spectra of urine from rats administered all treatments (see Table 1) were plotted with 60-cm horizontal expansions, and the peak height intensities of 16 endogenous urinary metabolites were measured at their assigned chemical shifts (Table 2). For metabolites with complex resonance patterns, such as glutamine and lysine, the maximum height of the multiplet was measured, giving a quantitative measure of the relative signal intensity. For each postdosing time point (0–8, 8–24, and 24–48 hr), metabolite peak heights were expressed relative to the corresponding peak height of TSP (taking account of the known TSP concentrations) and divided by the corresponding −24–0-hr predose value, and the resulting ratios were converted to $\log_{10}$ values. The mean $\log_{10}$ values for each metabolite for each animal treatment group were used to construct a time-course data set. A maximum-effect data set was compiled by recording the most positive or negative $\log_{10}$ value in the time-course data set, thus including the largest increase or decrease in the intensity of each TSP-corrected metabolite peak height over 48 hr. GER values derived for each animal by conventional clinical chemical methods were used as a second, independent, standard and were obtained as described in our earlier studies (2, 9–12). In this case, metabolite peak heights were expressed as GER-corrected ratios derived from comparison of the NMR peak height of each metabolite with that of the α-anomeric proton of glucose (see Table 2).

Computer PR analysis of scored and quantitative ^{1}H NMR-derived metabolite excretion data. Data handling and analysis were performed using the table generation and manipulation software RS/1 (BBN Software Products UK Ltd., Staines, Middlesex, UK) and the multivariate statistics package ARTHUR (version 4.1; B and B Associates, Seattle, WA), running on a DEC VAX 8550 computer. Control data were included where appropriate to the type of analysis. Before PR analysis, data were autoscaled to have a mean of 0 and unit variance and were analyzed directly by NLM and PCA procedures. Intertoxin metabolite correlation matrices were also calculated such that the principal diagonal elements equaled 1.0 and all other values reflected intertoxin correlations. Correlation matrices were analyzed after the calculation of scaled data, based on the subtraction of the overall mean of the matrices ("$r - \bar{r}$"). In this situation, data were not autoscaled before PR analysis. The metabolites that contributed most to separating the individual time points for a given site of nephrotoxic action (preclassified independently by histopathology) were determined through the calculation of variance or Fisher weights (5), with probabilities being assessed by paired Student's *t* tests.

Results

^{1}H NMR Spectroscopic Analysis of Urine from Nephrotoxin-Treated Rats

Typical ^{1}H NMR spectral profiles representing alterations in the excretion of various low molecular weight metabolites over a 48-hr time course after exposure to the S_1/S_2 segment-directed proximal tubular nephrotoxin CPH are illustrated in Fig. 1. A characteristic pattern of metabolite changes consistent with proximal tubular damage was clearly associated with CPH administration, as reported in previous studies (11, 12), and included glycosuria, selective amino aciduria (alanine, lysine, valine, glutamine, and glutamate), and lactic aciduria. Examination of ^{1}H NMR spectra of urine obtained 0–8 hr after exposure of rats to 20 or 40 mg/kg TCTFP (Fig. 2) revealed that the excretion patterns of several metabolites changed in common with those observed in urine from CPH-treated rats at the same time point (Fig. 1). The NMR profiles obtained after both CPH and TCTFP administration also clearly resembled those generated in other NMR studies after treament with other proximal tubular nephrotoxins, such as PAP, HCBD, and UN (2, 9, 10). However, close examination of the spectra indicated that each nephrotoxin treatment produces a unique perturbed biochemical response, reflecting the different known sites of the nephronal lesion and the mechanisms of toxicity. For example, the considerable increases in the urinary excretion of acetoacetate and HB associated with both CPH and TCTFP administration were apparent from 8 to 24 hr in CPH-treated rats but were detected from 0 to 8 hr after 40 mg/kg TCTFP and were not present in spectra from rats exposed to the lower dose of TCTFP (Figs. 1 and 2).

^{1}H NMR-Derived Metabolite Scores and Peak Height Data

Scored data relating to the effects of CPH, DCVHC, TCTFP, and UN on the excretion patterns of 16 metabolites throughout 48 hr after dosing have been combined with equivalent scored data from earlier NMR toxicity studies and are presented in Table 3. Quantitative ^{1}H NMR-derived peak heights expressed as $\log_{10}$ values and corrected for TSP and GER are given in Tables 4 and 5, respectively. These data show that each nephrotoxin treatment induces characteristic changes in the metabolite excretion profile; however, it is difficult to determine the exact relationships between the treatments with CPH, DCVHC, TCTFP, and UN and those described previously (2,

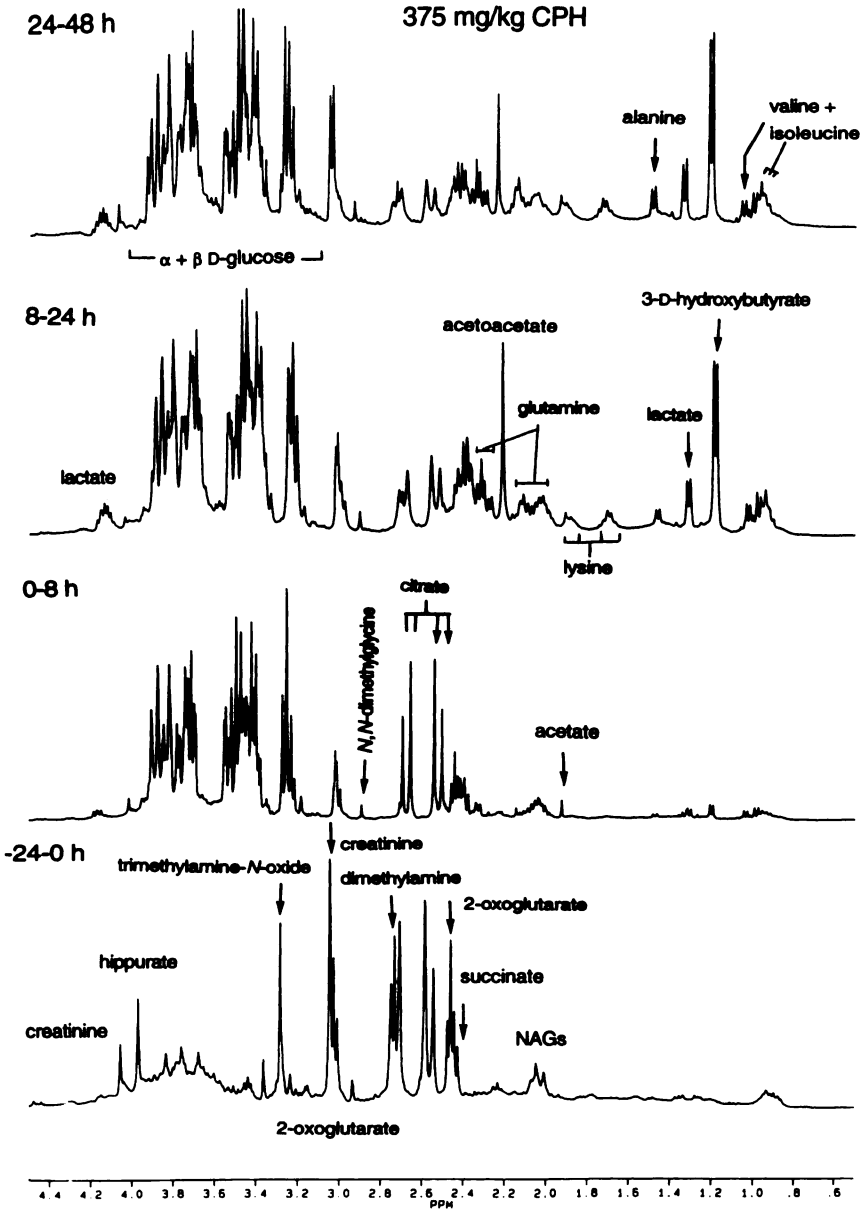

Fig. 1. Partial 400-MHz ^{1}H NMR spectra (low frequency region) of F344 rat urine before (−24–0 hr) and up to 48 hr after 375 mg/kg CPH administration. *Arrows*, points of peak height measurement. *NAGs*, indicates *N*-acetylated glycoprotein signals.

9, 10), either by visual inspection of the ^{1}H NMR spectra or by examination of the quantitative excretion profiles derived from the ^{1}H NMR data.

PR Analysis of ^{1}H NMR-Generated Metabolic Data

Semiquantitative scored data. The effect of examining the metabolite scores by NLM analysis and PCA is illustrated in Fig. 3. The NLM depicted in Fig. 3A was produced from the scored 16-dimensional maximum-effect data set (contained in Table 3); it showed only weak classification of the various nephrotoxicity states but separated the renal medullary toxins BEA and PI from the renal cortical toxin treatments. The control point was separate from all of the toxin treatments. PCA produced a tighter clustering of points than was observed in the NLM (Fig. 3A), with points for rats administered BEA and PI being more closely associated and distinct from those for the proximal tubular nephrotoxin treatments (Fig. 3B). The point for the S_1 segment nephrotoxin CrO_4^{2-} was further separated from the CPH points and the majority of the S_3 segment proximal tubular nephrotoxin treatment points. Of the latter, subclusters of points from rats treated with DCVHC and TCTFP and with the higher UN and CPH doses were apparent. Overall, PCA produced superior results, compared with NLM, in terms of the ability to discriminate between the sites of action of the various nephrotoxin treatments.

Because our previous studies (6, 7) indicated that taking the coefficients of determination between toxin treatments resulted in improved clustering of points, the effect of analyzing the maximum-effect scored data set by $r - \bar{r}$ correlation procedures was therefore also examined. The $r - \bar{r}$ PC plot illustrated in Fig. 3C revealed tighter clustering of related nephrotoxin treatments than was observed in the original PC plot (Fig. 3B). Points for rats administered BEA and PI were clearly distinct from the main cluster of points representing proximal tubular nephrotoxin treatments. Points representing rats exposed to DCVHC, TCTFP, HCBD, and PAP, which share a common mechanism of toxicity involving the formation of glutathione *S*-conjugates (see below), were closely associated in the $r - \bar{r}$

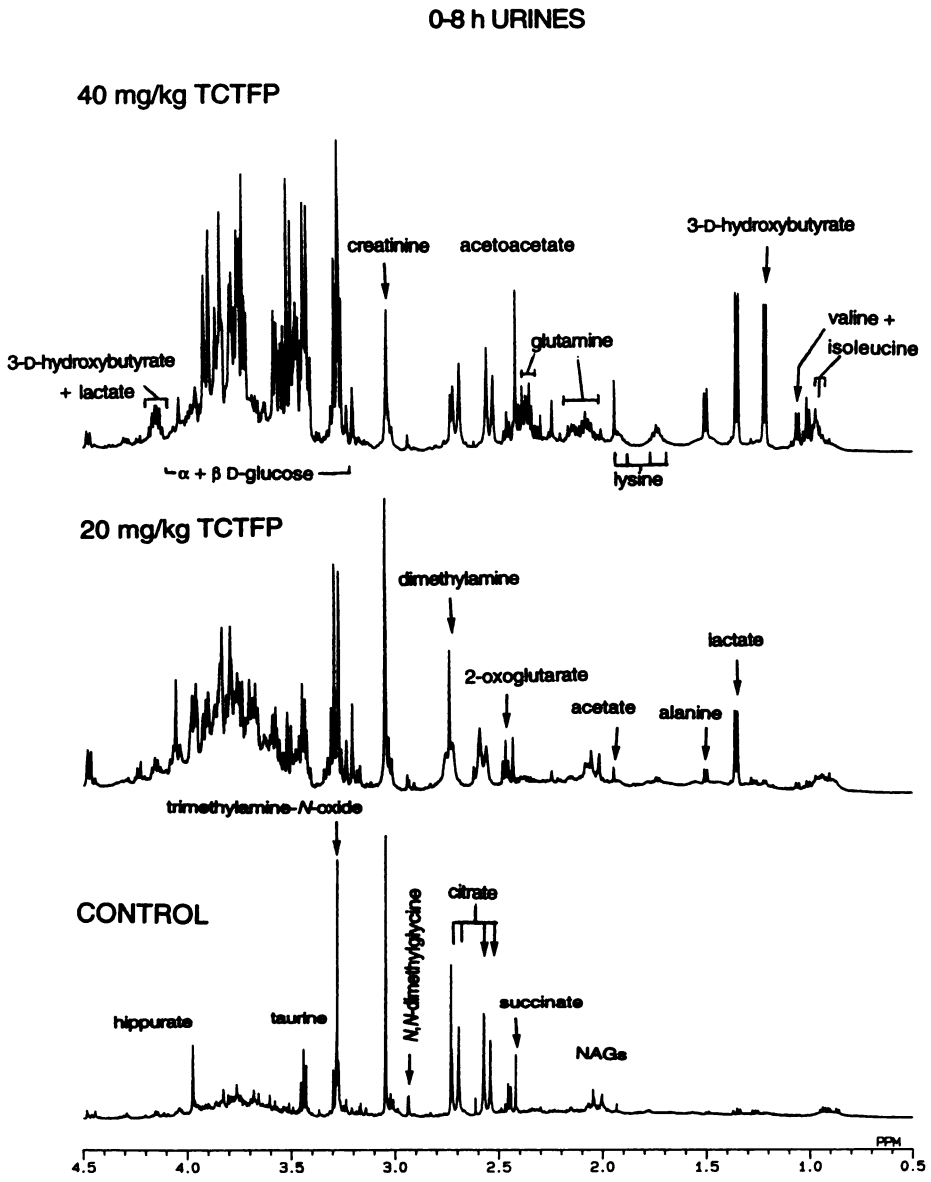

Fig. 2. Partial 400-MHz ^{1}H NMR spectra (low frequency region) of 0–8-hr urine samples obtained from a control F344 rat and from rats after administration of 20 and 40 mg/kg TCTFP. *Arrows*, points of peak height measurement. *NAGs*, indicates *N*-acetylated glycoprotein signals.

plot (Fig. 3C). Points representing the higher UN doses and 750 mg/kg CPH appeared similar, and the low dose UN treatment was associated with the remaining CPH doses and Hg^{2+}.

Correlation procedures ($r - \bar{r}$) were also applied to test whether they enhanced the analysis of the nephrotoxin treatments based on metabolite excretion scores occurring throughout all three time points. The overall clustering pattern observed with the maximum-effect data (Fig. 3C) was sustained after analysis of the 48-dimensional time-course data, with points for BEA- and PI-treated rats being clearly distant from those generated from rats administered the proximal tubular nephrotoxin treatments (Fig. 3D). However, improved separation of the CrO_4^{2-} treatment from the remaining proximal tubular toxin treatments was apparent after analysis of time-course information. The CPH and UN treatments were also better discriminated in the time-course map, although the point from rats treated with 750 mg/kg CPH remained distant from the other CPH doses. The existence of anticorrelation in the metabolite data set (data not shown) made comparison with $\bar{r}^2 - \bar{r}^2$ maps, as used previously (7), inappropriate. Overall, the inclusion of data from the additional toxin treatments maintained the classifications of site-specific nephrotoxicity that were described in our earlier study (7). Furthermore, the $r - \bar{r}$ approach of map generation from time-course data appeared to improve the classification of the site of toxicity of the compounds.

TSP-corrected peak height data. The PR approach was then extended by the use of quantitative peak intensity data to deduce the most appropriate method for NMR data preparation. The PC plot generated from TSP-corrected maximum-effect data revealed good discrimination between points from control, CrO_4^{2-}-treated, and renal medullary toxin-treated rats and those from rats administered the remaining proximal tubular toxin treatments (Fig. 4A). However, the point representing treatment with DCVHC mapped apart from the other S_3 segment proximal tubular treatments. The $r - \bar{r}$ PC plot generated from the same data set also distinguished points representing the BEA and PI treatments and CrO_4^{2-} from the remaining proximal tubular toxin treatments (Fig. 4B). In this case, the DCVHC, HCBD, PAP, and TCTFP treatments were

TABLE 3

^{1}H NMR-derived scored data portraying changes in the excretion patterns of 16 metabolites throughout 0–8 hr, 8–24 hr, and 24–48 hr after control or toxin treatments

See Materials and Methods for a description of the scoring system used. In each case, the first number represents the 0–8-hr modal value and the second and third numbers represent the 8–24-hr and 24–48-hr modal values, respectively.

	NMR scores														
	CPH (375 mg/kg)	CPH (750 mg/kg)	CPH (1500 mg/kg)	TCTFP (20 mg/kg)	TCTFP (40 mg/kg)	UN (5 mg/kg)	UN (10 mg/kg)	UN (20 mg/kg)	CrO_4^{2-}	Hg^{2+}	PI	HCBD	BEA	DCVHC	PAP	Control
Acetate	0, −1[a], −1	2, 1, 0	2, 1, −3	1, 1, 3	2, 0, 3	0, 1, 2	1, 0, 0	1, 2, 3	0, 0, 1	0, 1, 1	1, 2, 3	0, 1, 1	1, 2, 2	2, 2, 3	1, 1, 1	0, 0, 0
Alanine	1, 2, 2	1, 2, 2	1, 2, 2	1, 1, 2	2, 1, 1	0, 0, 1	0, 0, 0	1, 1, 2	0, 0, 1	0, 1, 1	0, 1, 1	0, 2, 2	0, 1, 1	2, 2, 1	2, 2, 2	0, 0, 0
HB	1, 3, 3	1, 3, 3	1, 3, 3	0, 2, 1	2, 3, 3	0, 0, 1	0, 2, 3	0, 2, 3	0, 0, 0	0, 0, 0	0, 0, 0	0, 1, 1	0, 0, 0	2, 2, 1	1, 1, 1	0, 0, 0
Creatinine	−2, −2, −2	−2, −2, −1	−3, −2, −2	0, −1, 0	−1, −2, −1	0, 0, −2	0, −2, −2	0, −2, −1	−1, −1, −1	−1, −1, −1	0, 0, 0	0, 0, 0	0, 0, 0	−2, −2, −2	−1, −1, −1	0, 0, 0
Citrate	0, −1, −1	0, −1, −2	0, −2, −2	−1, −2, −1	0, −2, −2	1, 0, −1	1, −2, −3	1, −1, −2	0, 0, 0	−1, −2, −3	0, 0, 1	0, 0, 0	0, −1, −2	−1, −2, −2	−1, −1, −2	0, 0, 0
Glucose	3, 3, 3	3, 3, 3	3, 3, 3	2, 3, 3	3, 3, 3	0, 3, 3	3, 3, 3	3, 3, 3	0, 0, 3	0, 2, 2	0, 0, 1	0, 3, 3	0, 0, 1	3, 3, 2	2, 3, 3	0, 0, 0
Glutamine	2, 2, 2	1, 2, 2	0, 1, 1	0, 2, 2	2, 1, 1	0, 2, 1	0, 2, 2	0, 2, 2	0, 0, 2	0, 1, 1	0, 0, 0	0, 2, 2	0, 0, 0	2, 1, 1	1, 2, 2	0, 0, 0
2-OG	0, −1, −1	−2, −2, −2	−1, −2, −2	−1, −2, −2	−1, −2, −2	1, 1, −1	1, −2, −2	1, −1, −2	0, 0, −1	−1, −2, −2	0, 0, −2	−1, 0, −1	0, −3, −3	−2, −3, −3	−1, −1, −1	0, 0, 0
Hippurate	−2, −3, −3	−3, −3, −3	−2, −2, −2	−1, −2, −2	−1, −2, −1	0, −2, −2	0, −3, −3	0, −3, −3	0, 0, −2	0, 0, −1	0, 0, 0	−1, −1, −3	0, 0, −1	−2, −2, −3	−1, −1, −1	0, 0, 0
Lactate	1, 2, 2	1, 3, 3	1, 2, 2	2, 3, 3	3, 2, 3	0, 1, 2	0, 2, 2	1, 2, 2	0, 0, 1	0, 2, 3	0, 1, 1	0, 2, 3	0, 1, 1	3, 3, 2	2, 2, 3	0, 0, 0
Succinate	−1, −1, −1	−1, 0, 0	−1, −2, −2	0, 0, 0	2, 0, 0	0, 0, 0	1, −2, −2	1, −2, −2	0, 0, −1	0, −1, −3	−1, 2, 3	0, 0, 1	−1, 1, 2	−1, −2, −2	1, −1, 1	0, 0, 0
Trimethylamine-*N*-oxide	0, 0, 0	0, 0, 0	−2, −2, −2	−1, −1, −1	0, −2, −2	0, 0, 0	−1, −1, −1	0, 0, 0	0, 0, 0	−1, −1, −2	2, 2, −3	0, 0, 0	2, −3, −3	−1, −2, −2	0, 0, 0	0, 0, 0
Valine	1, 2, 2	1, 2, 2	1, 2, 2	1, 2, 2	2, 2, 1	0, 0, 1	0, 1, 1	0, 1, 2	0, 0, 0	0, 1, 1	0, 0, 0	0, 2, 2	0, 0, 0	2, 1, 0	1, 2, 2	0, 0, 0
Dimethylamine	−3, −2, −2	−2, −3, −2	−2, −2, −2	1, −1, −1	−2, −2, −2	−2, −2, −2	−2, −2, −2	−2, −2, −2	0, 0, 0	0, −1, −1	2, 2, 1	0, 0, 0	2, 2, 1	−2, −2, −2	0, 0, 0	0, 0, 0
Lysine	1, 2, 2	1, 2, 2	0, 2, 2	1, 2, 2	2, 2, 1	0, 0, 1	0, 1, 1	0, 1, 2	0, 0, 1	0, 1, 1	0, 0, 0	0, 2, 2	0, 0, 0	2, 1, 0	1, 2, 2	0, 0, 0
DMG	−1, −1, −1	0, 1, 1	0, −1, −2	−1, −1, −1	0, −1, −1	0, 0, 0	0, 0, 0	0, 0, 0	0, 0, 0	−1, −1, 0	0, 0, 3	−1, −1, 0	0, 0, 3	−1, −1, −1	1, 0, 0	0, 0, 0

[a] Data used to construct maximum-effect PR maps are represented in bold.

more closely associated. Furthermore, although the CPH and UN points were close together, the CPH treatments were clearly clustered together. Application of correlation procedures to the analysis of the nephrotoxin treatments based on the inclusion of peak height time-course data (48-dimensional) resulted in inferior classifications of toxicity site, compared with the plot generated from maximum-effect data (Fig. 4B), in that, although the CPH treatments formed a subcluster, the clusters representing the BEA and PI treatments and the renal cortical treatments were less closely associated (Fig. 4C). Overall, these findings indicated that, both scored data, and peak height data resulted in classification of toxicity site. However, in contrast to scored data, the optimum procedure to discriminate the nephrotoxin treatments appeared to be an $r - \bar{r}$ correlation on the maximum-effect peak height data.

GER-corrected data. The $r - \bar{r}$ PC plot produced from GER-corrected maximum-effect data (Table 5) is illustrated in Fig. 5A. Points from BEA- and PI-treated rats were more closely associated than in the equivalent correlation map generated from TSP-corrected maximum-effect data (Fig. 4B), and the CrO_4^{2-} treatment point was also well separated. Points from rats administered the remaining proximal tubular nephrotoxin treatments were grouped together, with the DCVHC, HCBD, PAP, and TCTFP treatments being closely associated. The use of GER data provided an inferior separation of the CPH treatments, with the middle dose again appearing distant from the other two. The point for the middle dose of UN also mapped apart from the points for the remaining UN doses. The $r - \bar{r}$ PC plot derived from GER-corrected time-course data (48-dimensional) on the PR mapping positions demonstrated discrimination of the CrO_4^{2-} treatment from all other treatments (Fig. 5B). Points from BEA- and PI-treated rats were also separated from the proximal tubular treatments, although they were less closely associated with each other than was observed in the equivalent plot from maximum-effect data (Fig. 5A). Overall, the use of $r - \bar{r}$ correlation procedures with GER-corrected maximum-effect data (Fig. 5A) produced tighter clusters representing the different toxin treatment classifications than were observed with GER-corrected time-course data (Fig. 5B), confirming the findings with TSP-corrected peak height data.

Fisher weight and Student's *t* test analyses. Previous ^{1}H NMR studies have shown that region-specific nephrotoxicity results in the expression of characteristic urinary metabolite markers of toxicity (2, 11, 12). Inspection of ^{1}H NMR spectra of urine (2) and of NMR-derived data shown in Tables 3–5 clearly demonstrates that the perturbed metabolite profiles caused by proximal tubular toxins are different from the perturbations resulting from renal medullary toxicity. However, ^{1}H NMR spectra of rat urine from the various classes of renal cortical toxin treatments were markedly similar, as illustrated here with the S_1/S_2 segment proximal tubular toxin CPH and the S_3 segment proximal tubular toxin TCTFP (Figs. 1 and 2). Therefore, the use of PR techniques in discriminating the markers that separated the S_1, S_1/S_2, and S_3 segment classes of proximal tubular toxins was investigated, as was the potential of these techniques for revealing new information with respect to the onset and progression of nephronal damage. The 48-dimensional time-course data sets that contained $\log_{10}$ peak height data from many individual animals were used to calculate Fisher or variance weights, with comparisons being made

TABLE 4

TSP-corrected ^{1}H NMR-derived peak height data portraying changes in the mean excretion patterns of 16 metabolites throughout 0–8 hr, 8–24 hr, and 24–48 hr after control or toxin treatments

Data from each animal are expressed as a ratio to the predose (−24–0-hr) values, followed by logarithmic transformation. In each case, the first number represents the mean 0–8-hr value and the second and third numbers represent the 8–24-hr and 24–48-hr values respectively.

	TSP-corrected ratios							
	CPH (375 mg/kg)	CPH (750 mg/kg)	CPH (1500 mg/kg)	TCTFP (20 mg/kg)	TCTFP (40 mg/kg)	UN (5 mg/kg)	UN (10 mg/kg)	UN (20 mg/kg)
Acetate	**2.1,**[a] **1.8, 1.1**	**1.8, 1.3, −1.0**	**1.4, 1.1, 0.5**	**0.9, 1.7, 2.5**	**1.1, 1.9, 2.7**	**0.2, 1.0, 1.5**	**−0.04, 0.1, −0.04**	**0.4, 1.3, 1.4**
Alanine	**1.5, 1.9, 1.9**	**1.5, 1.7, 1.5**	**1.0, 1.5, 1.9**	**1.0, 1.9, 2.0**	**1.1, 2.2, 1.9**	**0.3, 0.9, 1.6**	**0.2, 0.3, 0.9**	**0.2, 0.9, 0.8**
HB	**1.8, 2.4, 2.1**	**1.8, 2.2, 2.0**	**1.0, 2.0, 2.3**	**0.9, 2.4, 2.1**	**1.4, 3.2, 3.0**	**−0.03, 0.9, 1.9**	**−0.3, 0.8, 2.1**	**0.3, 1.9, 2.0**
Creatinine	**0.9, 0.7, 0.5**	**0.3, 0.4, 0.2**	**0.6, 0.4, 0.6**	**0.4, 0.8, 0.9**	**0.5, 1.0, 0.9**	**0, 0.5, 0.6**	**−0.1, −0.1, 0.4**	**−0.2, 0.3, 0**
Citrate	**1.4, 0.7, 0.4**	**0.9, 0.4, −0.2**	**0.8, 0.1, −0.1**	**0.1, 0.4, 0.5**	**0.3, 0.6, 0.2**	**0.3, 0.6, 0.6**	**0.4, 0.05, −0.01**	**0, 0.2, −0.6**
Glucose	**2.4, 2.2, 1.9**	**1.8, 1.6, 1.1**	**1.8, 1.7, 1.8**	**1.0, 1.7, 1.6**	**1.2, 2.1, 1.6**	**0.3, 1.7, 1.9**	**0.4, 1.0, 1.8**	**0.5, 1.4, 0.9**
Glutamine	**2.1, 2.1, 1.6**	**1.4, 1.2, 0.9**	**1.2, 1.6, 1.6**	**0.9, 1.8, 1.8**	**1.0, 2.3, 2.3**	**0.2, 1.5, 1.9**	**0.1, 1.1, 1.8**	**0.5, 1.6, 1.3**
2-OG	**1.1, 0.7, 0.3**	**0.3, 0.2, −0.3**	**0.5, 0.04, 0.01**	**−0.1, 0.2, 0.7**	**0.1, 0.6, 0.1**	**0.3, 0.7, 0.7**	**0.6, 0.6, 0.9**	**0.2, 0.5, 0.03**
Hippurate	**0.1, −0.3, −0.3**	**0.2, −0.3, −0.7**	**0.1, −0.6, −0.8**	**0.2, 0.1, 0.1**	**0.1, 0.1, −0.4**	**0.1, 0.2, −0.3**	**0.2, −0.3, −0.5**	**−0.3, −0.2, −1.3**
Lactate	**1.6, 2.1, 1.8**	**1.5, 1.8, 1.4**	**1.2, 1.7, 1.8**	**1.2, 2.0, 2.0**	**1.2, 2.3, 2.0**	**0.2, 1.2, 2.0**	**0.2, 0.6, 1.3**	**0.1, 1.3, 1.2**
Succinate	**1.3, 1.2, 0.8**	**0.7, 0.5, 0.1**	**0.7, 0.6, 0.7**	**0.5, 0.6, 0.9**	**0.8, 1.2, 1.0**	**0.2, 0.7, 1.1**	**0.2, 0, 0.9**	**−0.2, 0.5, 0.2**
Trimethylamine-*N*-oxide	**1.4, 1.1, 0.9**	**1.0, 0.7, 0.3**	**0.7, 0.7, 0.7**	**0.3, 0.9, 0.9**	**0.4, 1.2, 0.9**	**−0.03, 0.4, 0.8**	**0.1, 0.5, 0.9**	**−0.2, 0.3, 0.1**
Valine	**2.0, 2.3, 2.0**	**2.0, 2.0, 1.8**	**1.3, 1.7, 2.0**	**1.2, 1.6, 2.0**	**0.7, 1.9, 1.7**	**0.4, 1.0, 1.8**	**0.04, 0.5, 1.5**	**0.1, 1.3, 1.1**
Dimethylamine	**0.4, 0.4, −0.1**	**0.4, −0.5, −0.4**	**−0.1, −0.3, −0.2**	**0.3, 0.3, 0.7**	**0.4, 0.1, 0.3**	**−0.3, 0.1, 0.1**	**−1.1, −0.4, −0.1**	**−0.3, 0.2, −0.1**
Lysine	**1.2, 1.9, 1.7**	**1.5, 1.7, 1.4**	**0.8, 1.4, 1.7**	**0.9, 1.7, 1.9**	**1.1, 2.3, 2.1**	**0.1, 1.0, 1.8**	**0.1, 0.5, 1.3**	**0.1, 1.2, 1.1**
DMG	**1.1, 1.0, 0.7**	**1.0, 0.9, 0.5**	**0.8, 0.7, 0.6**	**0.2, 0.7, 1.0**	**0.3, 0.9, 0.8**	**−0.1, 0.6, 0.7**	**−0.2, 0.1, 0.5**	**−0.3, 0.4, 0.1**

	TSP-corrected ratios							
	CrO_4^{2-}	Hg^{2+}	PI	HCBD	BEA	DCVHC	PAP	Control
Acetate	**−0.1, 0.3, 1.2**	**0.2, 2.1, 1.5**	**0.02, 0.6, 1.4**	**−0.04, 1.1, 1.5**	**1.0, 0.8, 1.3**	**1.2, 1.0, 0.8**	**1.3, 0.6, −0.02**	**−0.2, −0.01, 0.2**
Alanine	**−0.7, 0.4, 1.0**	**0.1, 1.7, 1.7**	**−0.2, 0.7, 0.3**	**0.1, 1.9, 2.1**	**0.5, 0.6, 0.5**	**1.6, 0.9, 0.2**	**1.7, 1.5, 1.3**	**−0.1, 0, 0.1**
HB	**0.4, 0.1, 0.5**	**0.1, 0.3, 0.8**	**−0.3, −0.1, −0.2**	**−0.04, 1.2, 1.3**	**0.3, −0.4, −0.5**	**1.5, 1.4, 0.5**	**1.7, 0.5, 0.1**	**−0.1, 0.03, 0.1**
Creatinine	**−0.03, 0.1, 0.3**	**−0.1, 0.4, 0.3**	**−0.1, 0.3, 0.2**	**0, 0.1, 0.4**	**0.5, 0.1, 0.5**	**0.1, −0.5, −1.0**	**0.7, −0.02, −0.03**	**−0.1, 0, 0.1**
Citrate	**0.2, 0.4, 0.5**	**0.01, −0.2, −0.1**	**−0.5, −0.1, −0.2**	**−0.2, −0.1, 0**	**0.4, −0.3, −0.6**	**0.3, −0.5, −1.9**	**0.5, −0.4, −0.8**	**−0.2, −0.04, 0.02**
Glucose	**−0.1, 0.4, 1.7**	**0.1, 1.4, 1.2**	**0.3, 0.8, 0**	**0.1, 1.8, 1.8**	**0.8, 0.5, 0.1**	**1.5, 0.9, −0.1**	**2.0, 1.6, 1.4**	**−0.1, 0.1, 0.2**
Glutamine	**−0.7, 0.4, 1.5**	**0.3, 1.3, 1.2**	**−0.1, 0.7, 0.4**	**0.1, 1.3, 1.2**	**0.7, 0.3, 0.1**	**1.5, 0.7, −0.03**	**1.7, 1.1, 0.8**	**0, 0, −1.0**
2-OG	**0.3, 0.6, 0.4**	**−0.1, −0.2, −0.9**	**−0.3, 0.1, 0**	**−0.3, 0.1, 0.2**	**0.1, −1.1, −0.8**	**−0.02, −0.8, −1.5**	**0.6, −0.2, −0.4**	**−0.3, −0.1, 0**
Hippurate	**−0.02, 0.03, −0.1**	**−0.2, −0.2, −0.4**	**−0.3, −0.01, −0.2**	**0.2, −0.3, −0.6**	**0.3, −0.3, 0.01**	**−0.1, −1.1, −1.9**	**0.3, −0.2, −0.4**	**−0.2, 0.02, 0.1**
Lactate	**−0.1, 0.05, 1.2**	**−0.2, 2.4, 2.1**	**−0.3, 0.8, 0.8**	**0.1, 2.0, 2.1**	**0.4, 1.1, 1.1**	**1.8, 0.4, 0.5**	**1.9, 1.5, 1.2**	**−0.1, 0.02, 0.1**
Succinate	**0.2, 0.4, 0.7**	**−0.2, 0.7, 0.1**	**−0.9, −0.5, 0.1**	**−0.2, 0.2, 0.4**	**−0.1, −0.5, −0.1**	**0.1, −0.3, −1.0**	**1.2, 0.3, 0.2**	**−0.3, 0.1, 0.03**
Trimethylamine-*N*-oxide	**−0.1, 0.1, 0.6**	**−0.2, −0.1, 0.1**	**−0.2, 0.1, −0.7**	**−0.04, 0.3, 0.4**	**0.3, −0.3, −0.3**	**0.5, −0.1, −1.1**	**1.0, 0.5, 0.2**	**−0.2, 0.02, 0.1**
Valine	**−1.5, 0.2, 0.7**	**0.6, 0.9, 1.0**	**0.01, 0.8, 0.1**	**−0.01, 1.6, 1.8**	**−0.1, 0.5, 0.3**	**1.4, 0.8, −0.2**	**1.4, 1.2, 1.0**	**−0.1, 0.1, 0.1**
Dimethylamine	**−0.5, −0.1, 0.1**	**−0.8, −0.3, −0.2**	**0, 0.3, 0.2**	**0.2, 0, 0.1**	**0.4, 0.1, 0.01**	**−0.2, −0.9, −1.7**	**0.8, 0.1, −0.2**	**−0.2, 0.01, 0.1**
Lysine	**0, 0.2, 0.8**	**0.04, 0.1, 1.1**	**0.2, 0.7, 0.3**	**0.2, 1.6, 1.8**	**1.3, 0.5, 0.01**	**1.4, 0.8, −0.3**	**1.7, 1.2, 0.9**	**−0.1, 0.1, 0.2**
DMG	**−0.2, 0.1, 0.6**	**−0.4, 0.5, 0.3**	**−0.4, −0.4, 0.03**	**−0.3, 0.3, 0.3**	**0.3, −0.4, −0.2**	**0.2, −0.2, −1.0**	**0.9, 0.2, −0.2**	**−0.4, 0.04, 0.1**

[a] Data used to construct maximum-effect PR maps are represented in bold.

TABLE 5

GER-corrected ^{1}H NMR-derived peak height data portraying changes in the mean excretion patterns of 16 metabolites throughout 0–8 hr, 8–24 hr, and 24–48 hr after control or toxin treatments

Data from each animal are expressed as a ratio to the predose (−24–0-hr) values, followed by logarithmic transformation. In each case, the first number represents the mean 0–8-hr value and the second and third numbers represent the 8–24-hr and 24–48-hr values, respectively.

	GER-corrected ratios							
	CPH (375 mg/kg)	CPH (750 mg/kg)	CPH (1500 mg/kg)	TCTFP (20 mg/kg)	TCTFP (40 mg/kg)	UN (5 mg/kg)	UN (10 mg/kg)	UN (20 mg/kg)
Acetate	**1.6**,[a] 1.1, 0.1	1.9, 1.3, **−2.3**	1.2, **1.4**, −0.1	0.5, 1.3, **2.2**	1.2, 1.4, **2.5**	0.4, 1.1, **1.7**	0.3, **0.9**, −0.6	1.0, 1.7, **1.9**
Alanine	1.0, **1.4**, 1.3	**1.6**, 1.6, 1.4	0.8, 1.7, **1.8**	0.6, 1.6, **1.7**	1.4, **1.8**, 1.7	0.5, 1.0, **1.8**	0.6, **1.1**, 1.1	0.8, **1.3**, 1.3
HB	1.4, **1.9**, 1.6	1.9, **2.1**, 2.0	0.8, **2.3**, 2.2	0.5, **2.1**, 1.8	1.5, **2.8**, 2.8	0.2, 0.9, **2.0**	−0.1, 1.9, **2.5**	0.9, 2.3, **2.5**
Creatinine	**0.4**, 0.2, −0.1	**0.3**, 0.3, 0.1	0.4, **0.6**, 0.5	−0.04, **0.6**, 0.6	0.6, 0.6, **0.8**	0.2, 0.6, **0.7**	0.3, **0.8**, 0.5	0.5, **0.7**, 0.5
Citrate	**0.9**, 0.2, −0.2	**1.0**, 0.3, −0.3	**0.6**, 0.3, −0.2	−0.4, 0.1, **0.2**	**0.4**, 0.2, 0	0.5, 0.6, **0.7**	**0.8**, 0.8, 0.1	**0.6**, 0.6, 0.1
Glucose	**2.0**, 1.7, 1.3	**1.8**, 1.6, 1.0	1.5, **2.0**, 1.7	0.5, **1.4**, 1.3	1.3, **1.7**, 1.4	0.6, 1.7, **2.1**	0.8, 1.8, **1.9**	1.1, **1.8**, 1.4
Glutamine	**1.6**, 1.6, 1.0	**1.5**, 1.1, 0.8	1.0, **1.9**, 1.6	0.4, **1.5**, 1.4	1.1, 1.9, **2.1**	0.4, 1.5, **2.0**	0.4, 1.8, **1.9**	1.1, **2.0**, 1.8
2-OG	**0.6**, 0.2, −0.2	**0.4**, 0.1, −0.3	**0.4**, 0.3, −0.1	**−0.5**, −0.1, 0.3	**0.2**, 0.2, −0.1	0.5, **0.8**, 0.8	1.0, **1.3**, 1.0	0.8, **0.9**, 0.5
Hippurate	−0.3, −0.8, **−0.9**	0.3, −0.3, **−0.8**	−0.03, −0.4, **−0.8**	−0.2, **−0.3**, −0.2	0.2, −0.4, **−0.6**	0.1, **0.2**, −0.2	0.2, **0.5**, −0.4	0.3, 0.2, **−0.8**
Lactate	1.2, **1.6**, 1.2	1.6, **1.7**, 1.3	1.0, **1.9**, 1.7	0.8, **1.7**, 1.7	1.3, **1.9**, 1.8	0.4, 1.3, **2.1**	0.6, 1.3, **1.5**	0.8, **1.8**, 1.7
Succinate	**0.8**, 0.7, 0.2	**0.8**, 0.4, 0.1	0.6, **0.9**, 0.6	0.04, 0.3, **0.6**	**0.9**, 0.8, 0.8	0.4, 0.8, **1.2**	0.6, 0.8, **1.0**	0.5, **0.9**, 0.7
Trimethylamine-*N*-oxide	**0.9**, 0.6, 0.3	**1.0**, 0.6, 0.3	0.6, **0.9**, 0.7	−0.1, **0.6**, 0.6	0.5, **0.7**, 0.7	0.2, 0.5, **0.9**	0.5, **1.2**, 1.0	0.4, **0.8**, 0.5
Valine	**1.6**, 1.6, 1.4	**2.1**, 2.0, 1.7	1.1, **1.9**, 1.9	0.7, **1.7**, 1.7	1.4, 2.0, **2.1**	0.3, 1.0, **1.9**	0.4, 1.3, **1.6**	0.7, **1.7**, 1.7
Dimethylamine	−0.02, −0.1, **−0.6**	0.4, **−0.5**, −0.5	**−0.6**, −0.1, −0.2	−0.1, 0, **0.3**	**0.6**, −0.2, 0.2	−0.1, 0.1, **0.2**	**−0.7**, 0.3, 0.1	0.4, **0.6**, 0.4
Lysine	0.8, **1.4**, 1.1	**1.6**, 1.6, 1.3	0.6, **1.6**, 1.6	0.5, 1.4, **1.5**	1.2, 1.8, **1.9**	0.3, 1.0, **1.9**	0.5, 1.3, **1.4**	0.7, **1.6**, 1.6
DMG	**0.6**, 0.5, 0.1	**1.0**, 0.8, 0.4	0.6, **0.9**, 0.5	−0.2, 0.4, **0.6**	0.5, 0.5, **0.6**	0.1, 0.6, **0.8**	0.2, **0.8**, 0.7	0.4, **0.8**, 0.5

	GER-corrected ratios							
	CrO_4^{2-}	Hg^{2+}	PI	HCBD	BEA	DCVHC	PAP	Control
Acetate	0.02, 0.5, **1.4**	0.3, **2.3**, 1.5	0.1, 0.5, **1.5**	0.1, 1.2, **1.6**	0.2, **0.6**, 0.4	**1.4**, 1.4, 1.1	**1.3**, 1.1, 0.4	**−0.2**, −0.1, 0.02
Alanine	−1.0, 0.6, **1.3**	0.3, **1.9**, 1.6	−0.1, **0.6**, 0.4	0.3, 2.0, **2.1**	−0.2, **0.4**, −0.3	**1.7**, 1.3, 0.5	1.6, **2.0**, 1.7	**−0.4**, −0.1, −0.1
HB	0.3, 0.4, **0.7**	0.3, −0.1, **0.7**	−0.3, −0.4, **−0.6**	0.1, 1.3, **1.4**	0.1, **−1.0**, 0	1.6, **1.7**, 0.8	**1.6**, 1.0, 0.5	**−0.3**, −0.1, −0.2
Creatinine	0.1, 0.3, **0.6**	0.1, **0.5**, 0.2	−0.04, 0.2, **0.3**	0.2, 0.2, **0.5**	−0.3, −0.1, **−0.4**	0.2, −0.2, **−0.7**	**0.6**, 0.5, 0.1	**−0.2**, −0.1, −0.1
Citrate	0.3, 0.6, **0.8**	0.2, −0.02, **−0.9**	**−0.4**, −0.2, −0.1	−0.1, **0.2**, 0.04	−0.4, −0.6, **−1.4**	0.5, −0.1, **−1.6**	**0.4**, 0.2, −0.4	**−0.3**, −0.1, −0.1
Glucose	−0.02, 0.3, **2.0**	0.3, 0.7, **1.2**	0.3, **0.7**, 0.1	0.2, **1.9**, 1.9	0.1, 0.2, **−0.7**	**1.6**, 1.3, 0.2	**1.9**, 2.2, 1.9	**−0.2**, 0, 0.1
Glutamine	−1.0, 0.6, **1.6**	0.5, **1.5**, 1.0	0, 0.4, **0.5**	0.3, **1.5**, 1.2	0.02, 0.03, **−0.8**	**1.6**, 1.0, 0.2	1.7, 1.6, 1.3	**−0.2**, −0.1, −0.1
2-OG	0.5, **0.8**, 0.7	0.1, 0, **−1.0**	−0.2, 0, **0.4**	−0.1, **0.2**, 0.2	−0.6, −1.3, **−1.6**	0.1, −0.5, **−1.2**	**0.5**, 0.3, 0.02	**−0.4**, −0.2, −0.2
Hippurate	0.1, **0.2**, 0.2	−0.03, −0.04, **−0.5**	**−0.2**, −0.1, −0.1	0.1, −0.4, **−0.8**	−0.4, −0.6, **0.8**	0, −0.7, **−1.7**	0.2, **0.3**, 0.04	**−0.3**, −0.1, −0.04
Lactate	0.04, 0.2, **1.5**	0, **2.6**, 2.0	−0.2, 0.6, **0.9**	0.2, 2.1, **2.2**	−0.3, **0.9**, 0.3	**2.0**, 1.8, 0.8	1.9, 2.0, 1.7	−0.1, 0.02, −0.02
Succinate	0.3, 0.6, **1.0**	0, **0.8**, 0.01	**−0.8**, −0.7, 0.3	−0.1, 0.3, **0.4**	−0.8, −0.7, **−0.9**	0.3, 0.04, **−0.7**	1.1, 0.8, 0.6	**−0.3**, −0.1, −0.1
Trimethylamine-*N*-oxide	0.1, 0.3, **0.9**	−0.03, **0.1**, 0.1	−0.2, 0, **−0.6**	0.1, 0.4, **0.5**	**−0.5**, −0.5, −1.2	0.6, 0.2, **−0.9**	0.9, **1.0**, 0.7	**−0.3**, −0.1, −0.1
Valine	**−2.1**, 0.4, 1.0	0.2, **1.3**, 1.0	−0.1, **0.6**, −0.02	−0.3, 1.7, **1.8**	**−0.7**, 0.2, 0.04	0.9, **1.1**, 0.1	**1.8**, 1.8, 1.5	**−0.7**, 0.02, −0.04
Dimethylamine	**−0.4**, 0.1, 0.4	**−0.6**, −0.1, −0.3	0.1, 0.1, **0.3**	**0.3**, 0.1, 0.1	−0.3, −0.2, **−0.9**	−0.1, −0.5, **−1.4**	**0.8**, 0.6, 0.3	**−0.2**, −0.1, −0.04
Lysine	0, 0.4, **1.1**	0.2, −0.4, **1.0**	0.1, **0.5**, −0.1	−0.7, 1.7, **1.9**	0.2, 0.1, **−0.8**	**1.6**, 1.1, −0.1	1.5, **1.6**, 1.4	**−0.2**, 0.1, 0.02
DMG	−0.1, 0.3, **0.9**	−0.2, **0.7**, 0.2	−0.3, **−0.5**, 0.1	−0.1, **0.4**, 0.3	−0.4, −0.6, **−1.1**	0.4, 0.1, **−0.8**	**0.8**, 0.7, 0.3	**−0.4**, −0.04, −0.1

[a] Data used to construct maximum-effect PR maps are represented in bold.

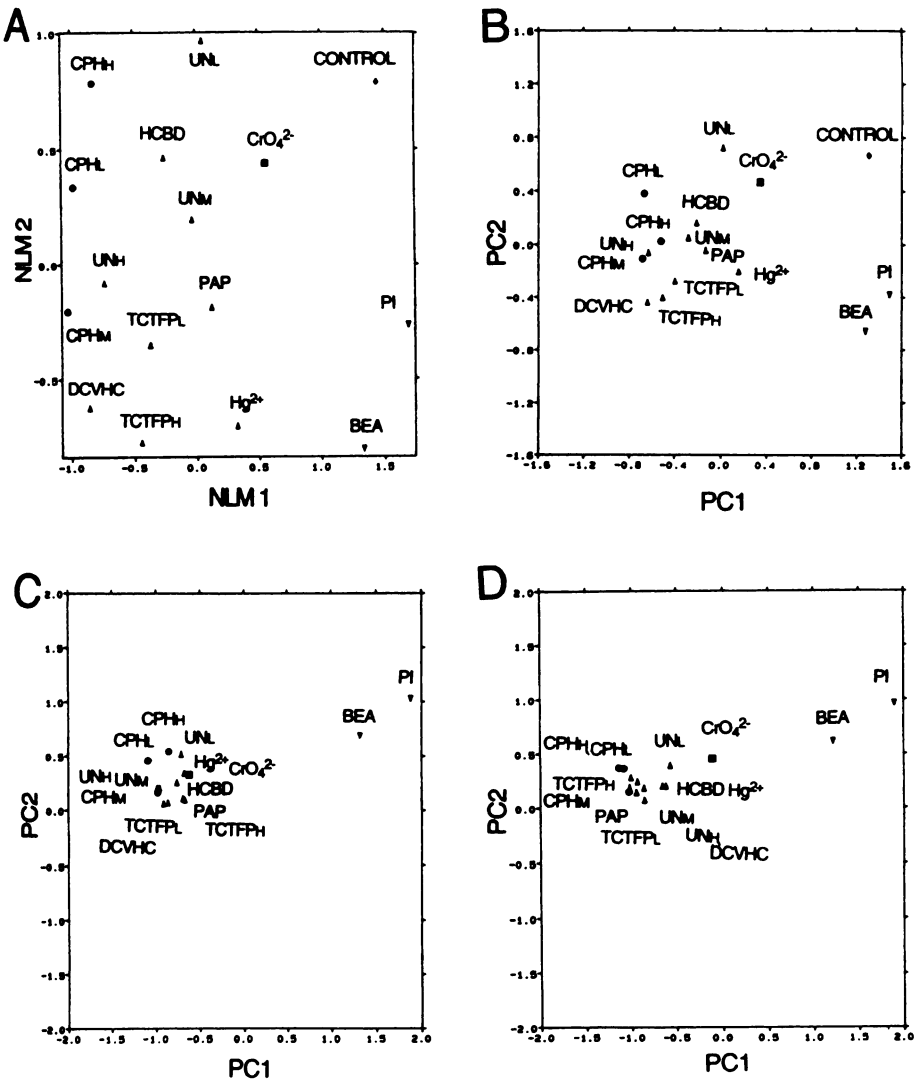

Fig. 3. Maps produced from the scored data given in Table 3. A, NLM of the maximum-effect scores; B, plot of PC1 versus PC2 for the maximum-effect scores; C, plot of PC1 versus PC2 for the $r - t$ correlation matrix of the maximum-effect scores; D, plot of PC1 versus PC2 for the $r - t$ correlation matrix of the time-course scores. Each *point* represents one toxin treatment. The percentage variance explained by the PCs is as follows: B, PC1, 55.9; PC2, 16.4; C, PC1, 77.2; PC2, 15.0; D, PC1, 77.3; PC2, 11.8. Data for A and B were autoscaled before analysis, whereas data for C and D were not autoscaled. Control data were omitted from C and D before analysis. *L*, lowest dose of toxin; *M*, middle dose of toxin; *H*, highest dose of toxin. Treatments were as follows: ♦, control; ▲, S_3 segment of proximal tubule; ▼, renal medulla; ●, S_1/S_2 segment of proximal tubule; ■, S_1 segment of proximal tubule.

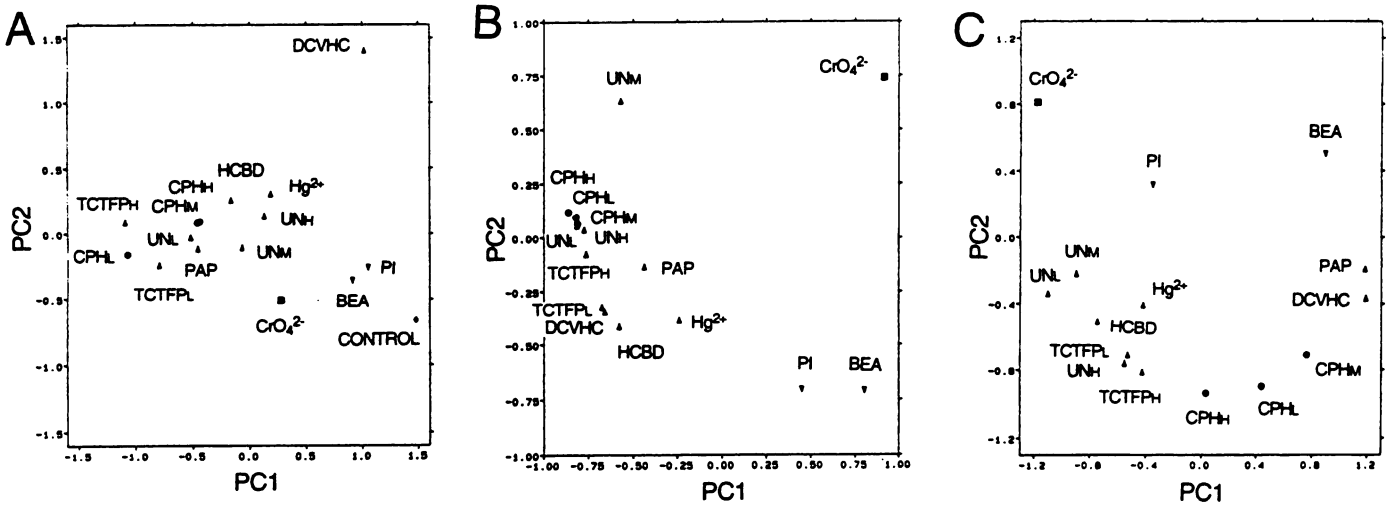

Fig. 4. Maps produced from the TSP-corrected peak height data given in Table 4. A, Plot of PC1 versus PC2 for the maximum-effect peak heights; B, plot of PC1 versus PC2 for the $r - t$ correlation matrix of the maximum-effect peak heights; C, plot of PC1 versus PC2 for the $r - t$ correlation matrix of the time-course peak heights. Data for A were autoscaled before analysis, whereas data for B and C were not autoscaled. Control data were omitted from B and C before analysis. The percentage variance explained by the PCs is as follows: A, PC1, 57.3; PC2, 19.8; B, PC1, 60.1; PC2, 21.0; C, PC1, 50.2; PC2, 29.1. Treatments were as defined in the legend to Fig. 3.

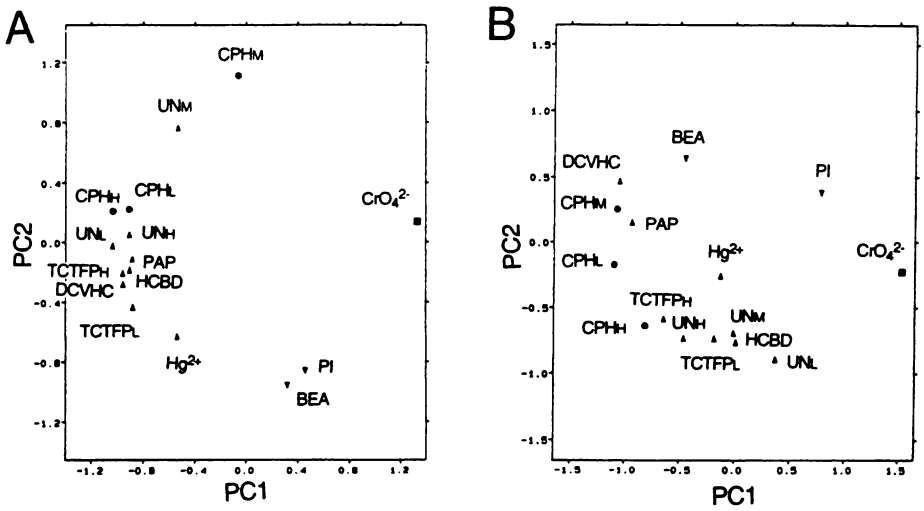

Fig. 5. Maps produced from the GER-corrected peak height data given in Table 5. A, Plot of PC1 versus PC2 for the $r - f$ correlation matrix of the maximum-effect peak heights; B, plot of PC1 versus PC2 for the $r - f$ correlation matrix of the time-course peak heights. Data were not autoscaled and control data were omitted before analysis. The percentage variance explained by the PCs is as follows: A, PC1, 67.1; PC2, 14.4%; B, PC1, 54.3; PC2, 22.6. Treatments were as defined in the legend to Fig. 3.

at each time point between the three proximal tubular toxin treatment groups. For many metabolites a Fisher weight of >5 was observed, suggesting good discriminating ability for these; however, there were some discrepancies between Fisher weight values according to which quantitation standard had been used. Although the actual value of a Fisher weight is not always diagnostic and there is no *a priori* reason for expecting the same values, a paired *t* test supported the proposal that certain metabolite values were significantly different ($p < 0.001$) between the three nephrotoxin classes under study. Whereas Fisher or variance weights involve intergroup comparisons, the paired *t* test retains intra-animal differences.

The most discriminating metabolites with respect to separating the three categories of proximal tubular toxins are presented in Table 6. It was apparent that for TSP- and GER-corrected peak heights 19 and 16 metabolite measurements respectively, were significant in the separation of one proximal tubular class from another and that several metabolites were common to both standardization methods. A combination of metabolite changes over the 48-hr study duration, incorporating greater excretion of glucose, HB, and amino acids (alanine, valine, and lysine), in concert with decreased excretion of hippurate and 2-OG, appeared to be involved in the discrimination of both the S_1/S_2 and S_3 segment-directed nephrotoxins from CrO_4^{2-} (the S_1 segment-directed nephrotoxin). In contrast, a different combination of metabolites were responsible for the separation of CPH (the S_1/S_2 segment-directed nephrotoxin) from the S_3 segment proximal tubular treatments. In this case, early (0–8 hr after dosing) decreases in the excretion of acetate, glucose, and DMG were observed after CPH treatment, relative to the S_3 segment proximal tubular treatments. The majority of the 16 metabolites at the three time points were necessary to separate the renal cortical, renal medullary, and control treatments (data not shown). Additional maps generated from the selected significant metabolites resembled those produced from the full metabolite data sets.

TABLE 6

List of urinary metabolites that differed most significantly between the proximal tubular nephrotoxin treatments, and direction of metabolite change over the 48-hr time course for both TSP- and GER-derived peak height data

Toxin categories	Metabolite	Time point	Fisher weight		Direction of change[a]
			TSP	GER	
		hr			
Proximal tubule, S_1 versus S_1/S_2	Glucose	0–8	18.2[b]	14.4[b]	+
	Valine	0–8	36.4[b]	25.3[b]	+
	DMG	0–8	10.2[b]	3.2	+
	Alanine	8–24	13.2[b]	14.0	+
	HB	8–24	37.1[b]	27.7[b]	+
	Citrate	8–24	0.1	6.8[b]	−
	Glucose	8–24	14.7[b]	24.7	+
	2-OG	8–24	0.4	14.2[b]	−
	Hippurate	8–24	3.6	7.0[b]	−
	Valine	8–24	20.9[b]	23.0[b]	+
	Lysine	8–24	18.6[b]	42.1[b]	+
	HB	24–48	11.0	7.4[b]	+
	Hippurate	24–48	0.8	9.1[b]	−
Proximal tubule, S_1 versus S_3	Glucose	0–8	1.5[b]	2.1	+
	Valine	0–8	7.3[b]	11.1[b]	+
	Lysine	0–8	0.8[b]	0.4	+
	Alanine	8–24	2.3[b]	4.8	+
	HB	8–24	1.5[b]	1.6[b]	+
	2-OG	8–24	0.6[b]	0.5	−
	Valine	8–24	3.1[b]	8.9	+
	Lysine	8–24	2.0[b]	1.8[b]	+
	HB	24–48	1.2	1.4[b]	+
	Hippurate	24–48	0.6	2.0[b]	−
	Valine	24–48	0.8	0.8[b]	+
Proximal tubule, S_1/S_2 versus S_3	Acetate	0–8	2.3[b]	0.9	−
	Glucose	0–8	2.2[b]	1.1	−
	DMG	0–8	2.0[b]	0.7	−

[a] Direction of change (+, increase; −, decrease) of significant metabolites of the second nephrotoxin class versus the first nephrotoxin class listed for each comparison.

[b] $p < 0.001$ (paired *t* test).

Discussion

^{1}H NMR spectra of urine and other biofluids contain data of considerable biochemical significance, and measurement of a suitable combination of metabolites can enable the classification of a toxic lesion in rats given different toxin treatments (1, 2, 13). Biochemical alterations in the urinary metabolite profile after administration of proximal tubule-directed nephrotoxins such as CPH and TCTFP include glycosuria, L-lactic aciduria, and selective amino aciduria (Figs. 1 and 2). In contrast, renal medullary toxins notably produce elevations in

urinary DMG, succinate, and acetate concentrations and decreased trimethylamine-*N*-oxide and 2-oxoglutarate excretion (2, 13). However, more subtle ^{1}H NMR-detectable metabolite changes, which may be equally important in classifying toxicity, may be overlooked easily. A major objective of the present work was to find the most efficient and reliable means of classifying ^{1}H NMR-generated toxicological data sets by use of PR methods and to seek new biochemical marker information for the detection of nephrotoxicity.

Evaluation of PR procedures and data preparation methods. The PR methods described have been applied to ^{1}H NMR data expressed both as scores and as quantitative peak heights. PCA produced a tighter clustering of points and hence an improved discrimination of proximal tubular nephrotoxin treatments from renal medullary toxin treatments than was observed after NLM analysis (Fig. 3), confirming earlier reports (7). This was attributed to the fact that PCA selects primary variance present in the input data sets, in contrast to NLM analysis, which considers all of the variance, including "noise" (5, 7). The two quantitation standards used produced comparable results, which validated the use of TSP as a standard in PR studies, although maps derived from GER data were slightly more consistent, in that tighter clustering of both the renal medullary toxin treatments and the S_1/S_2 and S_3 segment proximal tubular nephrotoxin treatments was apparent (Figs. 4 and 5). For absolute metabolite quantitation by NMR. TSP still poses problems as a standard in samples with high protein contents because of variable line-broadening effects.

Taking the ratio of peak heights to predose control values in the same animals, followed by logarithmic transformation, decreased the effect of inherent biological variability and approximated the seven-level scoring system where metabolite signal intensities were scaled to the theoretical control values, which are 0. The additional logarithmic transformation of those peak height data provided a normalized data distribution through a reduction in the variance typical of the larger ratios (14). Such preprocessing of data was crucial when implementing correlation procedures, because it reduced the otherwise undue influence a few high ratios would have had on the value of r. The generation of $r - \bar{r}$ maps revealed tighter clustering of related toxin treatments than was observed after direct mapping of the original data (Figs. 3 and 4). In maps generated directly from the original data, values were autoscaled before analysis so that each parameter was weighted equally and therefore had equal influence on the map. Autoscaling was not used before correlation map production because it can reduce correlation by introducing random deviations. The effect of error in the data was particularly important for data sets where many or all of the values were close to 0, because preliminary work demonstrated that such data could give random map positions, leading to misleading conclusions. Control data, being of this type, were therefore excluded from $r - \bar{r}$ mapping. It is also likely that the use of peak heights allowed the more subtle variations in metabolite concentrations, which could have been overlooked in the relatively coarse scoring system, to be incorporated in the PR analysis. Such variations had the potential to affect the PR mapping positions and hence the classifications of the various nephrotoxicity states, particularly in correlation maps.

Toxicological significance of applying the ^{1}H NMR-PR approach to urinalysis data. It is a characteristic feature of PR analysis that points that appear close together on maps have similar input values (5, 7), and this was used to assess the toxicological significance of the maps. Nephrotoxin treatments that altered the ^{1}H NMR spectral profiles in a similar manner would be expected to map close together and hence would be alike in terms of their toxicity (site of action). The PR maps were stable to the inclusion of the additional scores and a good classification of the site of nephrotoxicity was maintained, with the proximal tubular nephrotoxin treatments being clearly dissimilar from the renal medullary toxin treatments (Figs. 3 and 4). Conversion of data to correlation-related dimensions achieved a tighter discrimination of the toxin treatments (Figs. 3–5). Use of the maximum-effect scored data classified the nephrotoxins on the basis of their predominant site of toxicity; however, the separation of toxins that specifically affected the different regions of the proximal tubule (in particular, the S_1/S_2 and S_3 segments) was only partly achieved in the PR maps. For example, CPH affects the S_1/S_2 segments of the proximal tubule, as assessed by renal histopathology 48 hr after dosing (11), and is therefore distinct from the remaining proximal tubular toxins that affect the S_3 segment (12). However, many of the biochemical parameters of nephrotoxic damage are known to be common to CPH and the S_3 segment proximal tubular toxins (15), and this may partially account for some of the close associations between data points observed in many of the maps. It is also possible that using the maximum-effect data sets (containing data representing the largest metabolic changes) alone could have obscured any more subtle mechanistic information that may have been present in the time-course data sets, which possessed the highest dimensionality (i.e., 48 descriptors). Indeed, points describing the CPH data appeared to form a tighter group in the time-course maps (Fig. 3D), where they were distinct from the points for UN. The time-course maps also demonstrated some separation of CPH from several of the other S_3 segment proximal tubular toxin treatments. Of the S_3 segment nephrotoxin treatments, TCTFP and DCVHC, which share a common toxicity mechanism believed to involve GSH conjugation and toxic thiol production (16, 17), were closely associated in all maps, which suggests that the ^{1}H NMR metabolite data contained latent mechanistic information. The observation that the PAP and HCBD treatments, which also share this mechanism (18, 19), clustered away from CPH or the metal salts (UN or Hg^{2+}) supports this. New multivariate methods that can analyze such situations of embedded groups with similar mean values but different variances are becoming available (20, 21).

The general classifications of region-specific nephrotoxicity obtained after analysis of the scored data sets were maintained after PR analysis of the peak heights. The proximal tubular nephrotoxin treatments were generally well separated from the renal medullary ones, and points representing the control and CrO_4^{2-} treatments clustered apart from points for all other treatments. Correlation procedures transferred the outlying point from DCVHC-treated rats, apparent in maps generated directly from the peak height data, to a position near those of the other GSH *S*-conjugate-producing xenobiotics i.e., TCTFP, PAP, and HCBD (Fig. 4). This can be partially explained by considering DCVHC as a separate dose of an *S*-conjugate-producing xenobiotic, so that correlation eliminated the dose dependency and allowed site-specific effects to become more apparent. However, despite possessing the highest original dimensionality (i.e., 48), the time-course peak height data sets

did not yield the optimal discrimination of nephrotoxin treatments. The $r - \bar{r}$ correlation PC plots of maximum-effect peak height data provided the optimal indication of the site of nephrotoxic lesion.

An important aspect of the present study involved deriving the optimal methods by which the combination of metabolite markers required for the proximal tubular toxin classifications could be deduced. Analysis of the NMR-derived metabolite descriptors that were significant in peak height time-course data sets suggested that sufficient information was present to allow separation of the three proximal tubular nephrotoxin categories (Table 6). Combinations of several metabolites (including increases in glucose, HB, and amino acid excretion up to 24 hr after dosing, followed by decreases in the excretion of hippurate, citrate, and 2-OG from 24 hr after dosing) were significant in the separation of CPH and the S_3 segment proximal tubular toxin class from CrO_4^{2-}, the S_1 segment proximal tubular toxin (Table 6). Changes in the excretion of citric acid cycle intermediates such as citrate and 2-OG after administration of S_1/S_2 and S_3 segment-directed xenobiotics have been discussed previously (2, 10, 11) and may be related to inhibition of mitochondrial enzymes. Glycosuria and the enhanced excretion of amino acids are both strong indicators of proximal tubular damage in general, being caused by impaired tubular reabsorption of these compounds. After treatment with CrO_4^{2-}, amino acid excretion is not altered to a great extent and glycosuria occurs only at 24–48 hr after dosing (2). Hence, the combinations of significant metabolites in the NMR spectral profiles of urine from rats treated with the S_1/S_2 and S_3 segment toxin treatments, compared with CrO_4^{2-}, suggested by PR methods (Table 6) appear to closely parallel the development of the renal changes observed. The elucidation of markers of S_1/S_2 segment damage, compared with S_3 segment damage, is of considerable interest because the biochemical changes induced by administration of such toxins are so similar. The present findings suggest that early decreases in only three metabolites (acetate, glucose, and DMG) discriminated CPH from the S_3 segment treatments at the arbitrary level of significance of $p < 0.001$ (Table 6). It is of course possible that the ^{1}H NMR spectral properties that would facilitate differentiation among CPH and the S_3 segment nephrotoxins may include combinations of metabolites that were not measured in this study.

In summary, the coupling of ^{1}H NMR spectroscopy with PR techniques is a powerful approach to further the understanding of the biochemical processes associated with different types of toxic injury. The data analysis methods described here have provided a means of toxicological classification in terms of site of nephrotoxicity, mechanism of action, and severity of renal lesion. It should be noted that studies such as this conducted at higher NMR field strengths, e.g., 600 or 750 MHz will produce increased spectral dispersion and sensitivity and hence yield greater metabolic information. The current advances in NMR applications and technology render these methods amenable to automation, which should facilitate a move away from the manual methods of spectral quantitation. Direct NMR data transfer either of total spectra or of data-reduced representations by network communication between the spectrometer computer and data analysis computer is under development (22, 23), and reduction of whole ^{1}H NMR spectral data sets to high-dimensionality metabolite descriptors may provide additional discrimination in toxicological and clinical studies in the future.

Acknowledgments

We thank the Science and Engineering Research Council and the Wellcome Foundation Ltd. for access to NMR and computing facilities. We also thank E. Rahr and Dr. K. P. R. Gartland for useful discussion.

References

1. Nicholson, J. K., and I. D. Wilson. High resolution proton magnetic resonance spectroscopy of biological fluids. *Prog. NMR Spectrosc.* **21**:449–501 (1989).
2. Gartland, K. P. R., F. W. Bonner, and J. K. Nicholson. Investigations into the biochemical effects of region-specific nephrotoxins. *Mol. Pharmacol.* **35**:242–250 (1989).
3. Seal, H. *Multivariate Statistical Analysis for Biologists.* Methuen and Co. Ltd., London, 101–102 (1968).
4. Chatfield, C., and A. J. Collins. *Introduction to Multivariate Analysis.* Chapman and Hall, London, 57–59 (1980).
5. Sharaf, M. A., D. L. Illman, and B. R. Kowalski. Exploratory data analysis, in *Chemometrics* (P. J. Elving and J. D. Winefordner, eds.), Vol. 82. John Wiley and Sons, Chichester, UK, 179–295 (1986).
6. Gartland, K. P. R., S. M. Sanins, J. K. Nicholson, B. C. Sweatman, C. R. Beddell, and J. C. Lindon. Pattern recognition analysis of high resolution ^{1}H NMR spectra of urine: a nonlinear mapping approach to the classification of toxicological data. *NMR Biomed.* **3**:166–171 (1990).
7. Gartland, K. P. R., C. R. Beddell, J. C. Lindon, and J. K. Nicholson. Application of pattern recognition methods to the analysis and classification of toxicological data from proton nuclear magnetic resonance spectroscopy of urine. *Mol. Pharmacol.* **39**:629–642 (1991).
8. Kriat, M., S. Confort-Gouny, J. Vion-Dury, M. Sciaky, P. Viout, and P. J. Cozzone. Quantitation of metabolites in human blood serum by proton magnetic resonance spectroscopy: a comparative study of the use of formate and TSP as concentration standards. *NMR Biomed.* **5**:179–184 (1992).
9. Gartland, K. P. R., F. W. Bonner, J. A. Timbrell, and J. K. Nicholson. The biochemical characterisation of *p*-aminophenol-induced nephrotoxic lesions in the F344 rat. *Arch. Toxicol.* **63**:97–106 (1989).
10. Anthony, M. L., K. P. R. Gartland, C. R. Beddell, J. C. Lindon, and J. K. Nicholson. Studies of the biochemical toxicology of uranyl nitrate. *Arch. Toxicol.* **68**:43–53 (1994).
11. Anthony, M. L., K. P. R. Gartland, C. R. Beddell, J. C. Lindon, and J. K. Nicholson. Cephaloridine-induced nephrotoxicity in the Fischer 344 rat: proton NMR spectroscopic studies of urine and plasma in relation to conventional clinical chemical and histopathological assessments of nephronal damage. *Arch. Toxicol.* **66**:525–537 (1992).
12. Anthony, M. L. High resolution NMR spectroscopic and pattern recognition approaches to the biochemical characterisation of experimental nephrotoxicity states. Ph.D. thesis, University of London (1993).
13. Holmes, E., F. W. Bonner, B. C. Sweatman, J. C. Lindon, C. R. Beddell, E. Rahr, and J. K. Nicholson. Nuclear magnetic resonance spectroscopy and pattern recognition analysis of the biochemical processes associated with the progression of and recovery from nephrotoxic lesions in the rat induced by mercury(II) chloride and 2-bromoethanamine. *Mol. Pharmacol.* **42**:922–930 (1992).
14. Dixon, W. J. Efficient analysis of experimental observations. *Annu. Rev. Pharmacol. Toxicol.* **20**:441–462 (1980).
15. Kluwe, W. M. Renal function tests as indicators of kidney injury in subacute toxicity studies. *Toxicol. Appl. Pharmacol.* **57**:414–424 (1981).
16. Vamvakas, S., E. Kremling, and W. Dekant. Metabolic activation of the nephrotoxic haloalkene 1,1,2-trichloro-3,3,3-trifluoro-1-propene by glutathione conjugation. *Biochem. Pharmacol.* **38**:2297–2304 (1989).
17. Lash, L. H., and M. W. Anders. Mechanism of *S*-(1,2-dichlorovinyl)-L-cysteine- and *S*-(1,2-dichlorovinyl)-L- homocysteine-induced renal mitochondrial toxicity. *Mol. Pharmacol.* **32**:549–556 (1987).
18. Wolf, C. R., P. N. Berry, J. A. Nash, T. Green, and E. A. Lock. Role of microsomal and cytosolic glutathione *S*-transferases in the conjugation of hexachloro-1:3-butadiene and its possible relevance to toxicity. *J. Pharmacol. Exp. Ther.* **228**:202–208 (1984).
19. Gartland, K. P. R., C. T. Eason, F. W. Bonner, and J. K. Nicholson. Effects of biliary cannulation and buthionine sulphoximine pretreatment on the nephrotoxicity of *para*-aminophenol in the Fischer 344 rat. *Arch. Toxicol.* **64**:14–25 (1990).
20. Rose, V. S., J. Wood, and H. J. H. Macfie. Single class discrimination using

principal component analysis (SCD-PCA). *Quant. Struct. Activity Relat.* **10**:359–368 (1991).
21. Rose, V. S., J. Wood, and H. J. H. Macfie. Generalized single class discrimination (GSCD): a new method for the analysis of embedded structure-activity relationships. *Quant. Struct. Activity Relat.* **11**:492–504 (1992).
22. Farrant, R. D., J. C. Lindon, E. Rahr, and B. C. Sweatman. An automatic data reduction and transfer method to aid pattern recognition analysis and classification of NMR spectra. *J. Pharm. Biomed. Anal.* **10**:141–144 (1992).
23. Spraul, M., P. Neidig, U. Klauck, P. Kessler, E. Holmes, J. K. Nicholson, B. C. Sweatman, S. R. Salman, R. D. Farrant, E. Rahr, C. R. Beddell, and J. C. Lindon. Automatic reduction of NMR spectroscopic data for statistical and pattern recognition classification of samples. *J. Pharm. Biomed. Anal.*, in press.

Send reprint requests to: J. K. Nicholson, Department of Chemistry, Birkbeck College, University of London, Gordon House, 29, Gordon Square, London WC1H 0PP UK.

Correction

The authors have discovered an inaccuracy in their data published for the chromosomal assignment for the human $GABA_A$ receptor $\beta 2$ subunit reported in the article by Hadingham *et al.* (Vol. 44, No. 6, pp. 1211–1218, 1993). It has now been determined that the assignment of the gene for the human $GABA_A$ receptor $\beta 2$ subunit to chromosome 6 (1) was erroneous, and that the $\beta 2$ subunit maps to human chromosome 5. It is of interest to note that two other $GABA_A$ receptor subunit genes, $\alpha 1$ (2) and $\gamma 2$ (3), have also been mapped to chromosome 5.

Reference

1. Hadingham, K. L., P. B. Wingrove, K. A. Wafford, C. Bain, J. A. Kemp, K. J. Palmer, A. W. Wilson, A. S. Wilcox, J. M. Sikela, C. I. Ragan, and P. J. Whiting. Role of the β subunit in determining the pharmacology of human γ-aminobutyric acid type A receptors. *Mol. Pharmacol.* **44**:1211–1218 (1993).
2. Buckle, V. J., N. Fujita, A. S. Ryder-Cook, J. M. J. Derry, P. J. Barnard, R. V. Lebo, P. R. Schofield, P. H. Seeburg, A. N. Bateson, M. G. Darlison, and E. A. Barnard. Chromosomal localisation of GABA-A receptor subunit genes: relationship to human genetic disease. *Neuron* **3**:647–654 (1989).
3. Wilcox, A. S., J. A. Warrington, K. Gardiner, R. Berger, P. Whiting, M. R. Altherr, J. J. Wasmuth, D. Patterson, and J. M. Sikela. Human chromosomal localization of genes encoding the $\gamma 1$ and $\gamma 2$ subunits of the γ-aminobutyric acid receptor indicates that members of this gene family are often clustered in the genome. *Proc. Natl. Acad. Sci. USA* **89**:5857–5861 (1992).